Mechanism and ultrasensitivity in Hedgehog signaling revealed by Patched1 disease mutations

Kostadin Petrov[a], Taciani de Almeida Magalhaes[a], and Adrian Salic[a,1]

[a]Department of Cell Biology, Harvard Medical School, Boston, MA 02115

Edited by K. Christopher Garcia, Stanford University, Stanford, CA, and approved January 7, 2021 (received for review April 9, 2020)

Hedgehog signaling is fundamental in animal embryogenesis, and its dysregulation causes cancer and birth defects. The pathway is triggered when the Hedgehog ligand inhibits the Patched1 membrane receptor, relieving repression that Patched1 exerts on the GPCR-like protein Smoothened. While it is clear how loss-of-function Patched1 mutations cause hyperactive Hedgehog signaling and cancer, how other Patched1 mutations inhibit signaling remains unknown. Here, we develop quantitative single-cell functional assays for Patched1, which, together with mathematical modeling, indicate that Patched1 inhibits Smoothened enzymatically, operating in an ultrasensitive regime. Based on this analysis, we propose that Patched1 functions in cilia, catalyzing Smoothened deactivation by removing cholesterol bound to its extracellular, cysteine-rich domain. Patched1 mutants associated with holoprosencephaly dampen signaling by three mechanisms: reduced affinity for Hedgehog ligand, elevated catalytic activity, or elevated affinity for the Smoothened substrate. Our results clarify the enigmatic mechanism of Patched1 and explain how Patched1 mutations lead to birth defects.

Hedgehog signaling | holoprosencephaly | mathematical modeling | ultrasensitivity

Hedgehog (Hh) signaling is an essential metazoan signaling pathway responsible for patterning and growth of many tissues during development, including the central nervous system, limbs, long bones, heart, and mesenchymal tissues of the craniofacial region (1, 2). Insufficient Hh signaling is implicated in numerous birth defects, including holoprosencephaly (HPE), the most frequent congenital malformation of the brain (3); conversely, excessive Hh signaling causes cancers such as medulloblastoma and basal cell carcinoma (4).

When the Hh pathway is inactive, the membrane protein Patched1 (PTCH1) (5), a member of the Resistance–Nodulation–Division (RND) family of small-molecule transporters (6), represses the downstream seven-spanning transmembrane domain (7TMD) protein Smoothened (SMO) (7, 8); this repression prevents activation of the cytoplasmic steps in Hh signal transduction. The Hh pathway is triggered by an Hh ligand, such as Sonic Hedgehog (SHH) in vertebrates (9–12), which binds PTCH1 on the surface of responding cells and inhibits it (13, 14). Hh ligands are doubly lipidated, modified with palmitate N-terminally and cholesterol C-terminally. The interaction between SHH and PTCH1 involves the extended palmitoylated N-terminal peptide of SHH (palm-SHH22) (15), the globular part of SHH, and the cholesterylated C-terminal peptide (16). Importantly, the palmitate-mediated interaction is necessary and sufficient for PTCH1 inhibition during signaling (15). As result of PTCH1 inhibition, SMO becomes active and relays signals to the cytoplasm, leading to activation of the GLI zinc-finger transcriptional activators (17, 18), which are responsible for turning on specific target genes.

In vertebrates, the signaling steps outlined above take place in primary cilia, which are required for Hh signaling (19). PTCH1 localizes to the ciliary base in unstimulated cells (20) and, upon binding SHH, it is internalized and removed from cilia. In contrast, SMO is excluded from cilia in unstimulated cells but accumulates in cilia upon activation (18, 21, 22), causing ciliary recruitment and activation of the downstream GLI proteins (17, 18).

A major unresolved question in Hh signaling is the mechanism of SMO repression by PTCH1. Signaling by vertebrate SMO can be separated into at least two required steps: 1) SMO activation and 2) SMO translocation to the cilium (18, 21, 22); it is unclear, however, which step occurs first and at which step(s) PTCH1 acts to inhibit SMO. SMO is directly activated by cholesterol (23, 24), which binds to its extracellular cysteine-rich domain (CRD) (21, 25–28) and to a site in the bottom portion of the 7TMD (29). The current hypothesis is that PTCH1 inhibits SMO by antagonizing its activation by cholesterol, though it is unclear whether PTCH1 acts on CRD-bound or 7TMD-bound cholesterol (23, 24, 29). Recent cryo-electron microscopy (cryo-EM) and biochemical analyses of PTCH1 support the idea that PTCH1 is a cholesterol transporter (30–34), although the direction of cholesterol transport and the mechanism of SMO repression remain unknown.

PTCH1 is targeted by numerous disease mutations. Loss-of-function (LOF) PTCH1 mutations relieve the inhibition exerted on SMO, leading to constitutive SMO activation; these mutations cause cancer, as exemplified by Gorlin syndrome, an inherited predisposition to cancers driven by excessive Hh signaling (35). Interestingly, there is also evidence for gain-of-function (GOF) PTCH1 mutations, such as the ones associated with HPE (36, 37), a condition caused by reduced Hh signaling during embryogenesis (3). GOF PTCH1 mutants remain poorly understood, although they have the potential to shed light on the mechanism by which PTCH1 represses SMO.

Here, we investigate how the PTCH1–SMO signaling module operates in the Hh pathway and how it is affected by GOF mutations

Significance

The Hedgehog signaling pathway is fundamental in animal development, controlling the size, morphology, and differentiation of tissues and organs. How Hedgehog signaling is evolutionarily tuned to produce different outputs is poorly understood. We use cell biology, mathematical modeling, and analysis of mutations causing birth defects to demonstrate that ultrasensitivity is a key signal-processing feature of the Hedgehog pathway, which can lead to different outputs. We explain ultrasensitivity by a mathematical model of Hedgehog signaling whereby the tumor-suppressor membrane protein Patched catalyzes the deactivation of the GPCR-like transducer Smoothened in primary cilia. The Sonic Hedgehog ligand binds and inhibits Patched, causing switch-like Smoothened activation. Our results clarify the regulation of the Patched–Smoothened module in normal signaling and in disease.

Author contributions: K.P. designed research; K.P. and T.d.A.M. performed research; K.P. contributed new reagents/analytic tools; K.P. analyzed data; and K.P. and A.S. wrote the paper.

The authors declare no competing interest.

This article is a PNAS Direct Submission.

[1]To whom correspondence may be addressed. Email: asalic@hms.harvard.edu.

This article contains supporting information online at https://www.pnas.org/lookup/suppl/doi:10.1073/pnas.2006800118/-/DCSupplemental.

Published February 1, 2021.

associated with HPE. We first develop microscopy-based functional assays for PTCH1, which we show can be used to accurately measure PTCH1 activity in single cells. We find that PTCH1 exerts its inhibitory activity on SMO like an enzyme displaying zero-order ultrasensitivity. We use our assays to demonstrate that Hh signaling is greatly reduced by PTCH1 mutants from HPE, explaining their causal role in disease. Interestingly, we distinguish three mechanisms by which PTCH1 GOF mutants dampen Hh signaling: 1) loss of affinity for SHH ligand, 2) enhanced "affinity" of the PTCH1 enzyme for its downstream target SMO, and 3) enhanced PTCH1 catalytic activity toward SMO. Based on quantifying SMO regulation by PTCH1 and by various small-molecule modulators, we propose that PTCH1 functions by catalyzing SMO deactivation in cilia, by antagonizing CRD-bound cholesterol. Our findings illuminate the mechanism of SMO inhibition by PTCH1 and clarify how GOF PTCH1 mutations cause HPE.

Results

Assaying PTCH1 Activity in Single Cilia. Traditional, bulk measurements of Hh pathway output obscure individual cellular responses, which may differ significantly from population averages. Furthermore, such differences can provide critical information on Hh signaling mechanism and dynamics and the functional impact of disease-causing mutations in Hh pathway components. To measure PTCH1 activity with single-cell resolution, we stably expressed PTCH1 in Ptch1$^{-/-}$ mouse embryonic fibroblasts (MEFs) (38), which display constitutive Hh signaling, with active SMO accumulating in primary cilia (17). We then measured the level of both PTCH1 and endogenous SMO in cilia, by fluorescence microscopy. This assay relies on two aspects of vertebrate Hh signaling: that PTCH1 operates in primary cilia to repress SMO (20) and that ciliary localization of SMO is a measure of its activity state (21, 22, 26, 28). Furthermore, this assay has the advantage that PTCH1 activity is measured by examining its immediate downstream target, SMO, in contrast to measuring a distant downstream readout such as transcriptional output. As expected, wild-type PTCH1 strongly reduced ciliary SMO (Fig. 1*A*), while two classical LOF PTCH1 mutants that cause Gorlin syndrome were defective (Fig. 1*A*), consistent with their significantly reduced ability to repress Hh signaling (39). Importantly, all PTCH1 constructs were properly targeted to cilia (*SI Appendix*, Fig. S1*A*).

Ciliary levels of PTCH1 are variable within each Ptch1$^{-/-}$ MEF population expressing PTCH1 transgenes (*SI Appendix*, Fig. S1*B*). We took advantage of this variability to ask whether

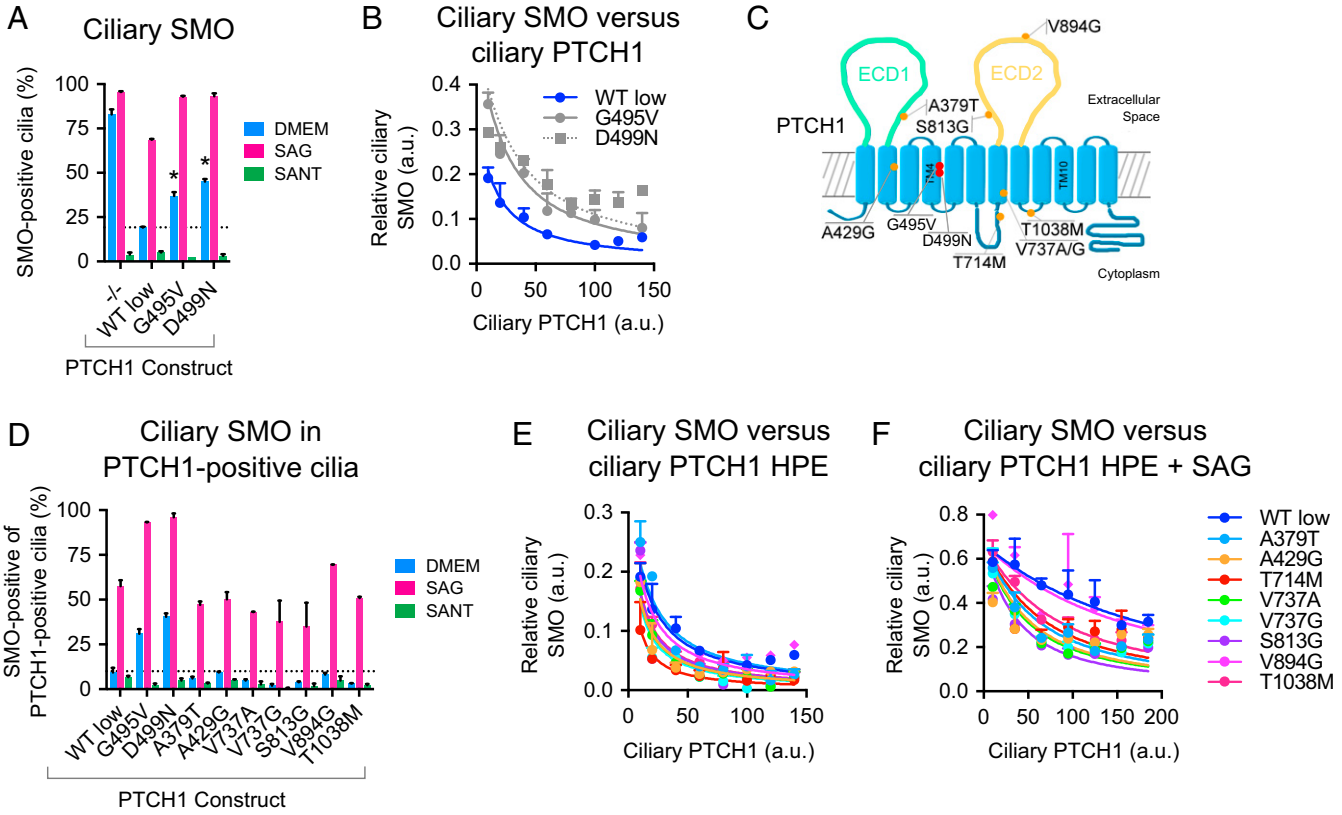

Fig. 1. Measuring PTCH1–SMO regulation with single-cilia resolution. (*A*) Wild-type PTCH1 or PTCH1 LOF mutants (G495V and D499N, mouse PTCH1 residue numbering) were stably expressed in Ptch1$^{-/-}$ MEFs, and endogenous SMO was measured in cilia. Wild-type PTCH1 reverses SMO accumulation in cilia, in contrast to LOF mutants. Incubation for 3 h with the SMO agonist SAG (0.1 μM) and the antagonist SANT1 (1 μM) serve as positive and negative controls for SMO activation and accumulation in cilia. (*B*) Correlation between ciliary PTCH1 and ciliary SMO in individual cilia show nonlinear repression of SMO by PTCH1. LOF PTCH1 mutants are defective in repressing SMO, as indicated by a shallower correlation than for wild-type PTCH1. Curves show fit to Eq. 3 (*SI Appendix, Supplementary Discussion*) with $\tau = 1$, and $k = 2$ for wild-type PTCH1 and $k = 1$ for LOF mutants. (*C*) Schematic of mouse PTCH1. ECD1 and ECD2 are the extracellular domains of the protein. Red dots indicate oncogenic LOF mutations, and yellow dots indicate mutations found in HPE. (*D*) As in *A*, but with stable expression of PTCH1 HPE mutants and showing SMO levels in PTCH1-positive cilia. Wild-type PTCH1 and all PTCH1 HPE mutants reverse SMO accumulation in cilia. See also *SI Appendix*, Fig. S1*C* for SMO levels in all cilia in this experiment. (*E*) As in *B*, but with PTCH1 HPE mutants. Most PTCH1 HPE mutants repress SMO more potently than wild-type PTCH1, as indicated by steeper ciliary SMO–PTCH1 correlations. The V894G mutant displays wild-type activity toward SMO. See also *SI Appendix*, Fig. S1*D* for pairwise comparison between wild type and individual PTCH1 mutants. (*F*) As in *E*, but in the presence of SAG (0.1 μM). SAG reduces responsiveness of SMO to PTCH1, allowing better separation between curves for wild-type and mutant PTCH1. See also *SI Appendix*, Fig. S1*E* for pairwise comparisons. (*A*–*F*) Data show mean of two biological replicates with associated SDs (*Student's *t* test $P < 0.05$).

levels of SMO and PTCH1 in individual cilia are correlated. As shown in Fig. 1*B*, we observed a dose-dependent decrease in ciliary SMO as a function of increased ciliary PTCH1. The correlation between ciliary SMO and PTCH1 levels was nonlinear, suggestive of PTCH1 acting catalytically to repress SMO (discussed below). Importantly, the correlation curve was shifted up for PTCH1 Gorlin mutants compared to wild-type PTCH1 (Fig. 1*B*), demonstrating the sensitivity of our assay to reduction in PTCH1 activity. The correlation we observed is reminiscent of the relationships between Hh pathway output and the amount of PTCH1 transiently transfected into Ptch1$^{-/-}$ cells, obtained using bulk transcriptional reporter assay (39).

Enhanced Activity of PTCH1 HPE Mutants. We next used our functional assay in Ptch1$^{-/-}$ MEFs to examine the activity of PTCH1 mutants associated with human HPE (Fig. 1*C*). All mutants localized to cilia (*SI Appendix*, Fig. S1 *A* and *B*) and completely reversed endogenous SMO accumulation in cilia, indicating that they are fully active in SMO repression (Fig. 1*D* and *SI Appendix*, Fig. S1*C*). Importantly, SMO retained responsiveness to the synthetic agonist, SAG (40), implying it remained functional in the presence of PTCH1 mutants (Fig. 1*D* and *SI Appendix*, Fig. S1*C*). To measure the strength of SMO repression by PTCH1 HPE mutants, we examined the correlation between ciliary SMO and PTCH1 levels. Strikingly, all but one of the mutants showed a correlation curve shifted down relative to wild-type PTCH1 (Fig. 1*E* and *SI Appendix*, Fig. S1*D*), suggesting that the majority of HPE mutants are hyperactive in repressing SMO. The remaining HPE mutant (V894G) displayed a correlation similar to wild-type PTCH1, indicating that the activity of this mutant toward SMO is unaffected. Importantly, the observed differences in activity were not due to differences in bulk PTCH1 expression, since PTCH1 and SMO levels were simultaneously measured in single cilia.

To further document the apparent increased activity of PTCH1 HPE mutants we measured the correlation between ciliary PTCH1 and SMO in the presence of large amounts of SAG. SAG binds to a site located in the upper portion of 7TMD of SMO (29, 41), distinct from the subjacent 7TMD cholesterol site (29, 42), leading to SMO activation and ciliary accumulation. Since SAG reduces sensitivity of SMO to PTCH1 (40), we reasoned that it should help reveal enhanced PTCH1 activity, against the already high activity of wild-type PTCH1. As expected, in the presence of SAG wild-type PTCH1 was less effective in reducing ciliary SMO, with the hyperbola-like SMO–PTCH1 curve shifted up (Fig. 1*F* and *SI Appendix*, Fig. S1*E*). Importantly, even in the presence of SAG all PTCH1 HPE mutants except V894G showed enhanced activity compared to wild-type PTCH1 (Fig. 1*F* and *SI Appendix*, Fig. S1*E*). Interestingly, cilia of Ptch1$^{-/-}$ MEFs contain only ~50% of maximal SMO (*SI Appendix*, Fig. S1*C*), defined as ciliary SMO levels induced by saturating SAG. This suggests that, in the absence of PTCH1, ciliary SMO accumulation is limited not by ciliary capacity but rather by the intrinsic SMO activation–inactivation equilibrium (discussed below).

Measuring PTCH1 Activity by Pharmacological Cross-Competition Assay in Single Cilia. Although the SMO-PTCH1 correlation assay was sufficient to detect enhanced activity of PTCH1 HPE mutants, we needed a more sensitive assay to better define how PTCH1 controls SMO and to dissect the effect of PTCH1 mutations. Specifically, we wanted to measure PTCH1 activity when the amount of active ciliary SMO is varied independently; this is similar to measuring enzymatic activity while varying substrate levels. To vary ciliary levels of endogenous SMO in a defined manner we treated cells simultaneously with SAG and the SMO antagonist SANT1 (40), both at saturating levels but at different ratios (SAG concentration was kept constant, while SANT1 concentration was varied). SAG and SANT1 compete for binding to SMO 7TMD (40, 43) and have opposite effects on SMO activity and ciliary localization (18, 21). We then measured ciliary SMO as function of the SANT1/SAG ratio, after an incubation time (3 h) sufficient for ciliary SMO levels to reach near-steady state (*SI Appendix*, Fig. S2*A*). We first performed these measurements in MEFs containing zero, one, or two copies of the Ptch1 gene (Fig. 2*A*). PTCH1 levels strongly influence the SMO response, such that higher PTCH1 levels shift the dose–response curve leftward and downward (toward lower SANT1/SAG ratios). Importantly, the responses of Ptch1$^{-/-}$, Ptch1$^{+/-}$, and Ptch1$^{+/+}$ MEFs are all well-separated (Fig. 2*A*), indicating that this assay, which we refer to as pharmacological cross-competition assay, accurately and sensitively reports on PTCH1 activity in cells.

Modeling SMO Dynamics Reveals that PTCH1 Antagonizes Both SMO Activation and Ciliary Accumulation. Activation of SMO requires at least two steps: adoption of the active conformation and localization to cilia (18, 21, 22). However, the sequence of steps is unclear, as is how PTCH1 affects these steps, to cause SMO repression. To address this question, we turned to mathematical modeling of SMO dynamics, with the goal of accounting for the data obtained with our cross-competition assay. We began with a simple model (*SI Appendix*, Model 1, Fig. S2*B*, and *Supplementary Discussion*), which assumes that 1) SMO exists in either repressed (SMO^{R}) or active (SMO^{A}) conformation and 2) SMO regulation occurs prior to ciliary entry. Under equilibrium conditions, assuming that SMO activation is faster than ciliary translocation, and that both are much slower that small-molecule binding kinetics, we obtain Eq. 1:

$$\frac{\mathrm{SMO_C}}{\mathrm{SMO_T}} = (1 + \beta(\alpha\rho(x) + 1))^{-1}. \quad [1]$$

Eq. 1 relates the fraction of total SMO concentrated in cilia ($\frac{\mathrm{SMO_C}}{\mathrm{SMO_T}}$) as a hyperbolic function of the SMO inactivation/activation equilibrium (parameter α), the SMO ciliary export/import equilibrium (parameter β), the ratio of SAG and SANT1 dissociation constants (parameter ρ), and the SANT1/SAG concentration ratio (variable x); because SAG and SANT1 dissociation constants are known (40), parameter ρ is defined to be ρ = 10. This model did not fit the cross-competition data (*SI Appendix*, Fig. S2*C*), as it did not account for the residual ciliary SMO observed at high SANT1/SAG ratios. We thus modified Model 1 to take into account regulation of SMO inside cilia (*SI Appendix*, Model 2, Fig. S2*B*, and *Supplementary Discussion*). Like Model 1, Model 2 assumes that SMO activation precedes import into cilia; however, Model 2 allows inactivation of ciliary SMO and export of inactive SMO from the cilium. Under equilibrium conditions, Model 2 leads to Eq. 2, which contains the additional parameter c, describing the speed of SMO ciliary trafficking relative to SMO activation:

$$\frac{\mathrm{SMO_C}}{\mathrm{SMO_T}} = \left(1 + \beta\frac{(1+\alpha)(1+\rho x) + c\rho x}{(1+\alpha\rho x)}\right)^{-1}. \quad [2]$$

Eq. 2 fits the cross-competition data well (*SI Appendix*, Fig. S2*C*), consistent with the idea that SMO inactivation occurs after ciliary entry and that inactive SMO is largely excluded from the ciliary compartment; thus, PTCH1 antagonizes both SMO activation (α) and ciliary accumulation (β) (Fig. 2*C*). Importantly, it is PTCH1 activity, and not the mere presence of PTCH1, that affects SMO ciliary dynamics: Both α and β are reduced for PTCH1 Gorlin mutants (*SI Appendix*, Fig. S2*E*), similar to what is observed in cells with reduced PTCH1 copy number (Fig. 2*C*).

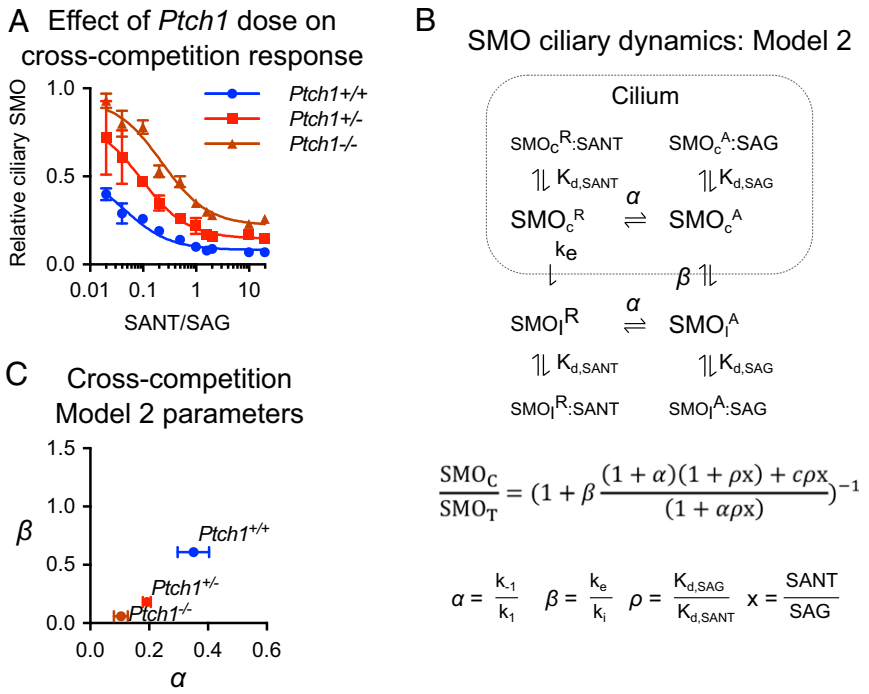

$$\frac{SMO_C}{SMO_T} = \left(1 + \beta \frac{(1+\alpha)(1+\rho x) + c\rho x}{(1+\alpha\rho x)}\right)^{-1}$$

$$\alpha = \frac{k_{-1}}{k_1} \quad \beta = \frac{k_e}{k_i} \quad \rho = \frac{K_{d,SAG}}{K_{d,SANT}} \quad x = \frac{SANT}{SAG}$$

Fig. 2. Cross-competition assay reveals PTCH1 antagonizes SMO activation and ciliary import, and PTCH1 HPE mutants are hyperactive. (*A*) Cross-competition response of SMO in MEFs with three different PTCH1 levels. Cells were incubated for 3 h in the presence of SANT1 and SAG at various ratios, and ciliary intensity of endogenous SMO was measured by immunofluorescence. Data show mean of two biological replicates with associated SDs; curves were fit to Eq. 2 with $\rho = 10$ and $c = 5$. (*B*) Model of SMO dynamics with pharmacological modulation by SAG and SANT1. Ciliary SMO levels (SMO_C) are governed by an activation/inactivation equilibrium (α) and an import/export equilibrium (β). Active SMO (SMO^A) can be imported and exported from the cilium, as well as converted to inactive SMO (SMO^R) in the cilium; in contrast, SMO^R is not imported into cilia and only subject to export. (*C*) SMO dynamic parameters extracted from fitting Eq. 2 to cross-competition data in *A*. PTCH1 dose affects α and β proportionately. Data show parameter estimates with associated SE of the estimate.

Majority of PTCH1 HPE Mutants Antagonize SMO More Potently than Wild-Type PTCH1. We used the pharmacological cross-competition as an additional assay to measure activity of PTCH1 HPE mutants. The results confirm that most PTCH1 HPE mutants are more potent than wild-type PTCH1 in repressing SMO (*SI Appendix*, Fig. S2 *D–F*), as previously suggested by the cross-correlation assay. Interestingly, HPE mutant potency correlates with disease severity: The A379T mutant, which shows a cross-competition response similar to wild type, was isolated from a mild semilobar HPE case (37), while the V737G/A and T1038M mutants, which show greatly increased potency, were isolated from severe HPE cases [alobar HPE with microcephaly (36, 37)]. Importantly, both α and β parameters are increased proportionally in HPE mutants (*SI Appendix*, Fig. S2*E*), further demonstrating that, irrespective of potency, PTCH1 antagonizes both SMO activation and ciliary accumulation. Finally, we note that activity differences between PTCH1 mutants cannot be attributed to differences in expression level, as our analysis was conducted in individual cilia, and only in cilia with detectable PTCH1. Indeed, cilia in the population without detectable PTCH1 showed responses characteristic of Ptch1$^{-/-}$ cells (*SI Appendix*, Fig. S2 *G* and *H*).

PTCH1 Inhibition by Ligand Causes Switch-Like Activation of SMO. We next used our single-cilia assay to ask how SMO responds to PTCH1 inhibition by ligand during Hh signaling. SHH binding causes both PTCH1 inhibition and internalization from cilia (15), the latter being dispensable for Hh pathway activation (15). Since PTCH1 internalization would affect ciliary PTCH1 measurements, we first assayed Hh signaling triggered by the palm-SHH22 peptide, which inhibits PTCH1 without removing it from cilia (15); thus, both PTCH1 and SMO can be simultaneously quantified in each cilium. To control for the effect of PTCH1 levels, we first performed measurements in two stable cell populations, one with low and another with high average wild-type PTCH1 levels (Fig. 3*A* and *SI Appendix*, Fig. S3 *A–D*). The dose–response data were fit to the Hill equation and estimates of effective concentration, 50% (EC_{50}) and Hill slope (n) were computed. This analysis yielded an EC_{50} for palm-SHH22 of 0.6 to 0.8 μM (Fig. 3*B*), a value consistent with our previous measurements by transcriptional reporter (15); the EC_{50} showed a small dependence on PTCH1 levels (Fig. 3 *A* and *B*), such that cells with low PTCH1 had a slightly lower EC_{50} than the cells with high PTCH1. Strikingly, we observed a Hill slope coefficient significantly greater than 1 ($n \approx 2$) (Fig. 3*B*), irrespective of PTCH1 expression levels. A similar Hill slope coefficient was obtained when high- and low-PTCH1 cells were stimulated with the palmitoylated SHH ligand (Fig. 3 *C* and *D*), which both inhibits and internalizes PTCH1. Furthermore, we confirmed that a Hill slope of $n = 2$ also occurs with endogenous PTCH1 levels, by quantifiying SMO activation by palm-SHH22 or palmitoylated SHH in wild-type MEFs (Fig. 3 *E–G*). Finally, a similar Hill slope was observed for cells treated with purified SCUBE2:SHH (Fig. 3 *H* and *I*), a complex consisting of palmitoylated and cholesterylated SHH bound to the extracellular chaperone SCUBE2 (16). Together, these results show that SMO activation during Hh signaling is switch-like, irrespective of PTCH1 level and inhibition mode.

Hyperactive PTCH1 HPE Mutants Have Altered Ligand Responses, Suggesting PTCH1–SMO Ultrasensitivity. The observed switch-like activation of SMO may be due to PTCH1 allostery, or to a PTCH1-SMO enzymatic system operating in an ultrasensitive regime. To distinguish between these possibilities and to determine how hyperactive PTCH1 HPE mutants affect Hh signaling we measured SMO activation by palm-SHH22 in Ptch1$^{-/-}$ MEFs reconstituted with these mutants (Fig. 4 *A–D*). The HPE mutants

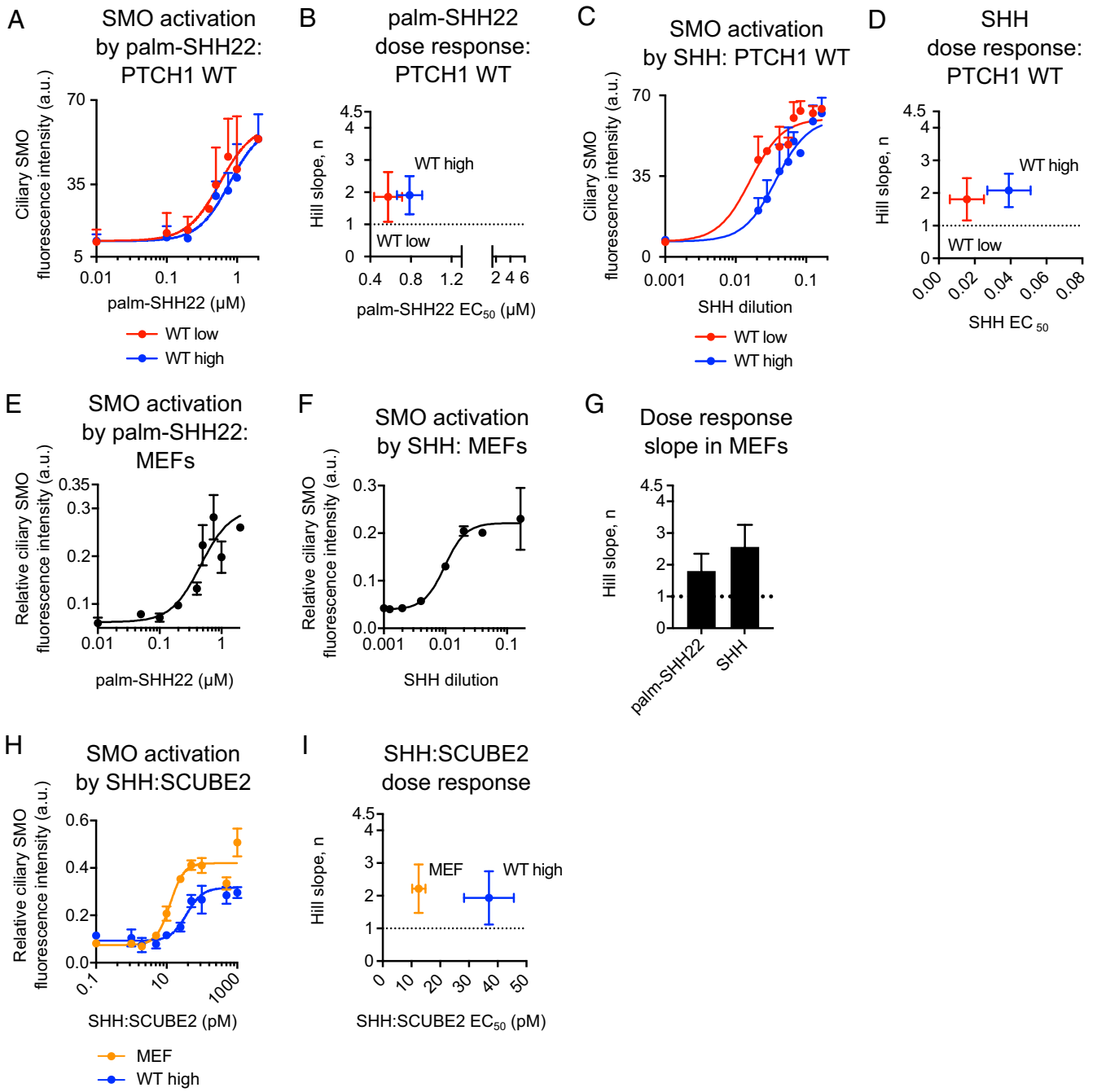

Fig. 3. PTCH1 inhibition by ligand induces switch-like activation of SMO. (*A*) Wild-type PTCH1 tagged with mCHERRY was stably expressed in Ptch1$^{-/-}$ MEFs, and high- and low-expressing populations were isolated by fluorescence-activated cell sorting. Accumulation of endogenous SMO in cilia was measured following a 3-h treatment with various doses of palm-SHH22 peptide. The response of SMO to PTCH1 inhibition by palm-SHH22 is switch-like (Hill slope n > 1) in both cell populations. Data show mean of two biological replicates with associated SDs; curves show fit to the Hill equation. (*B*) Hill equation parameters for the dose–responses in *A*. PTCH1 expression levels have a small effect on EC_{50} values and no effect on the Hill slope n ≈ 2. Data show parameter best-fit values with associated SE of the estimate after nonlinear, least-squares regression. (*C*) As in *A*, but cells were stimulated with various dilutions of conditioned media containing palmitoylated SHH. The response of SMO to PTCH1 inhibition by SHH is switch-like. (*D*) Hill equation parameters for the dose–responses in *C*. PTCH1 expression levels have an effect on EC_{50} values but no effect on the Hill slope n ≈ 2. Data show parameter best-fit values with associated SE of the estimate after nonlinear, least-squares regression. (*E*) As in *A*, but with wild-type MEFs. Median fluorescence intensity of ciliary SMO is normalized to maximal levels, defined as ciliary SMO after treatment with SAG (0.1 μM). Activation of SMO by palm-SHH22 is switch-like. (*F*) As in *A*, but wild-type MEFs were treated with palmitoylated SHH. Ciliary SMO was normalized as in *E*. (*G*) Hill slope parameter estimates from curves in *E* and *F*; error bars show SE of the estimate. (*H*) As in *A*, but wild-type MEFs and high PTCH1-expressing Ptch1$^{-/-}$ MEFs were treated with purified SCUBE2:SHH. Ciliary SMO was normalized as in *E*. SMO activation by SCUBE2:SHH is switch-like. (*I*) EC_{50} and Hill slope parameter estimates from curves in *H*; error bars show SE of the estimates.

have altered responses to palm-SHH22, and, interestingly, they segregate into two distinct subsets. Subset 1 mutants (V737G, V737A, and T1038M) show wild-type-like EC_{50} (Fig. 4*A*) but substantially higher Hill slope coefficient (n ≈ 3) (Fig. 4*D*). In contrast, Subset 2 mutants (A429G, T714M, S813G, and V894G) show elevated EC_{50} values (Fig. 4*B*) but wild-type-like Hill slope

coefficients (n ≈ 2) (Fig. 4*D*). Importantly, these mutant PTCH1 behaviors are not due to differences in expression level (*SI Appendix*, Fig. S3 *E* and *F*). Furthermore, as with the cross-competition assay, we observe a correlation between the severity of the molecular defect (EC_{50} or Hill slope) and clinical phenotype. The A379T mutant, with a mild phenotype, shows wild-type-like EC_{50} (Fig. 4*C*) and n (Fig. 4*D*), while the V737A/G and T1038M mutants, which have severe clinical phenotypes, show significantly elevated n values (Fig. 4 *B* and *D*).

That a subset of PTCH1 HPE mutations cause a significant increase in the Hill slope coefficient (n ≈ 3) of the SMO activation curve suggests that ultrasensitivity (i.e., a saturated PTCH1 enzyme), and not PTCH1 allostery, is the likely reason for the switch-like response of the PTCH1–SMO system to ligand (*Discussion*).

The Hyperactive PTCH1 HPE Mutants Are Not Defective in Ligand Binding. The reduced responsiveness to ligand of the hyperactive PTCH1 HPE mutants could be caused by defective ligand binding. To test for this possibility, we measured HPE mutant binding to unpalmitoylated SHH (which assays the interaction between PTCH1 and the globular part of SHH) and to palm-SHH22 (which assays the interaction between PTCH1 and the palmitoylated N terminus of SHH), and we assayed SHH-dependent internalization. All hyperactive PTCH1 HPE mutants bound unpalmitoylated SHH (Fig. 4*E* and *SI Appendix*, Fig. S3*H*) and palm-SHH22 (Fig. 4*F* and *SI Appendix*, Fig. S3*I*) with affinity comparable to that of wild-type PTCH1, and all of them exited cilia with SHH treatment (*SI Appendix*, Fig. S3*G*). These data indicate that ligand binding is normal for these PTCH1 HPE mutants, and thus their reduced sensitivity to ligand is likely a consequence of their enhanced inhibitory activity toward SMO (discussed below and in *Discussion*).

A Dynamical Model for Ultrasensitive PTCH1–SMO Regulation. To understand the switch-like response of wild-type PTCH1 to ligand and the behavior of hyperactive HPE mutants, we turned to mathematical modeling of PTCH1 as a Michaelis–Menten enzyme (Fig. 5*A* and *SI Appendix*, Model 3 and *Supplementary Discussion*). Briefly, since PTCH1 antagonizes both SMO activation and ciliary accumulation (Fig. 2*E*), we use a single rate parameter (catalytic constant, k_{cat}) to describe PTCH1 inhibition of active, ciliary SMO (SMO_C). Additionally, we assume that SMO undergoes PTCH1-independent activation/deactivation and ciliary trafficking, represented by the k_1 and k_{-1} rate constants. With respect to ligand, we restricted our model to palm-SHH22, because it inhibits PTCH1 without removing it from cilia (15); this reduces the dynamics of PTCH1 inhibition to a simple binding equilibrium, governed by the ligand dissociation constant K_d (Fig. 5*A*). Under equilibrium conditions, the model yields Eq. 3:

$$\frac{SMO_C}{SMO_T} = \frac{1-\tau(k+1)-\gamma PTCH1+\sqrt{4\tau(k+1)+(\tau(k+1)+\gamma PTCH1-1)^2}}{2(k+1)}. \quad [3]$$

Eq. 3 expresses the fraction of total SMO in cilia $\left(\frac{SMO_C}{SMO_T}\right)$ as a function of free PTCH1, and the parameters $k=\frac{k_{-1}}{k_1}$, $\tau=\frac{K_M}{SMO_T}$, and $\gamma=\frac{k_{cat}}{k_1 SMO_T}$. At equilibrium, in the presence of ligand, free PTCH1 is a function of ligand concentration (L) and ligand dissociation constant (K_d):

$$PTCH1 = PTCH1_T\frac{K_d}{K_d+L}. \quad [4]$$

Eq. 3 is an instance of a dynamical system, which produces two categories of responses: hyperbolic-like and ultrasensitive (44). The transition between these categories is governed by model

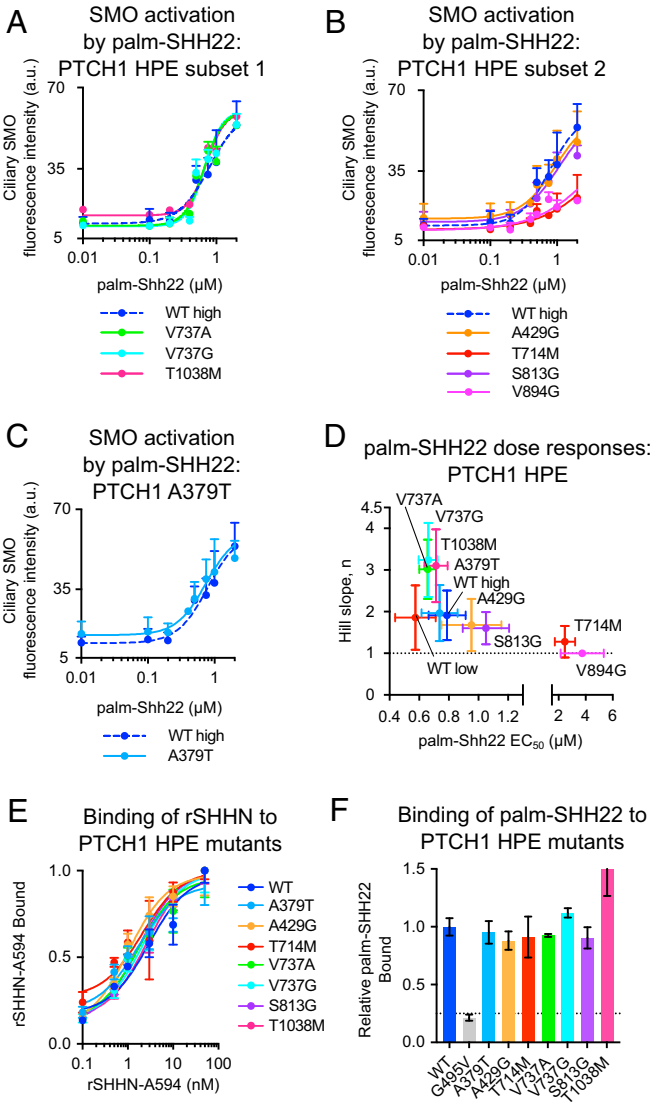

Fig. 4. PTCH1 HPE mutants have altered responses to ligand, caused by distinct mechanisms. (*A–C*) $Ptch1^{-/-}$ MEFs reconstituted with PTCH1 wild-type or HPE mutants were treated for 3 h with different amounts of palm-SHH22, and ciliary levels of endogenous SMO were measured. (*A*) Subset 1 HPE mutants have an elevated Hill slope (n ≈ 3) compared to wild-type PTCH1 (n ≈ 2). Data show mean of two biological replicates with associated SDs. (*B*) As in *A*, but with Subset 2 HPE mutants, which have an elevated EC_{50} relative to wild-type PTCH1. (*C*) As in *A*, but with HPE mutant A379T, which shows a response similar to wild-type PTCH1. (*D*) Estimates of Hill equation parameters for the dose–responses in *A–C*. Dotted line shows a Hill slope n = 1. Data show parameter best-fit value with associated SE of the estimate after nonlinear, least-squares regression. (*E*) Hemagglutinin-tagged PTCH1ΔC constructs (wild-type and HPE mutants) were expressed in HEK293T cells, and saturation binding of AlexaFluor594-labeled recombinant unpalmitoylated SHH (rSHH-A594) was measured by fluorescence microscopy. All HPE mutants show normal binding to rSHH. Data show mean of two biological replicates with associated SDs; curves show binding isotherm fits. (*F*) As in *E*, but with binding of fluorescent palm-SHH22. All HPE mutants show normal binding to the palmitoylated SHH N terminus The G495V mutant does not bind palm-SHH22 (15) and serves as negative control.

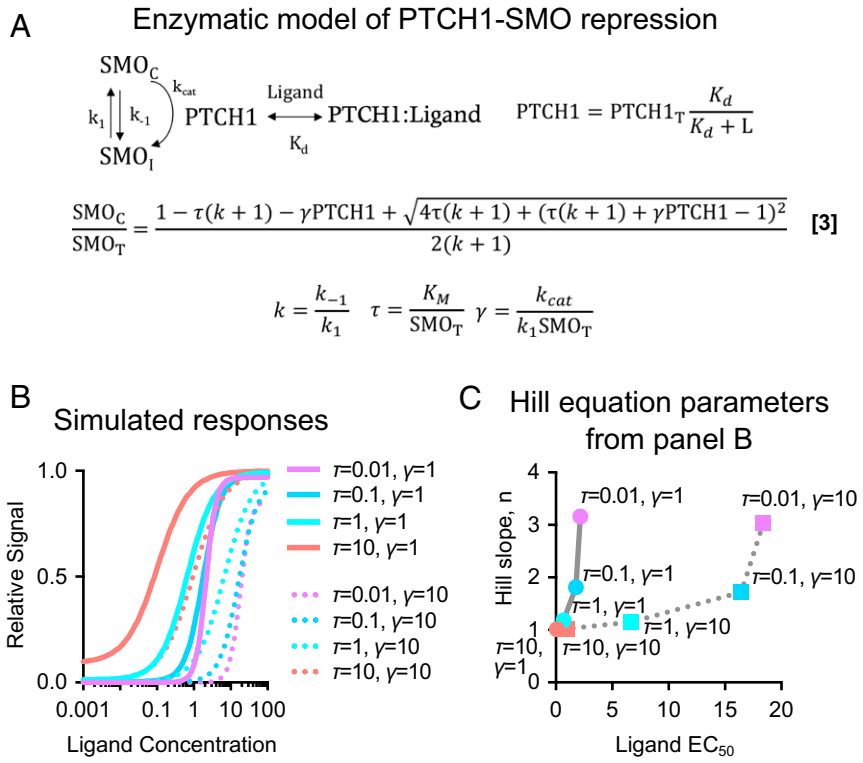

Fig. 5. Model of catalytic SMO regulation by PTCH1 predicts switch-like responses to ligand. (*A*) In the model, it is assumed that PTCH1 regulates SMO like a Michaelis–Menten enzyme, converting active, ciliary SMO (SMO_C) into nonciliary, inactive SMO (SMO_I). Apart from PTCH1-mediated regulation, SMO is also subject to an intrinsic activation/deactivation equilibrium expressed by the constant k. At equilibrium, the model yields Eq. 3 (*SI Appendix, Supplementary Discussion*), which expresses SMO_C as a function of free PTCH1. Parameter τ is a function of PTCH1 K_M, γ is a function of PTCH1 k_{cat}, and K_d is the ligand-PTCH1 dissociation constant. (*B*) Simulated ligand dose–responses according to Eqs. 3 and 4, with various values for τ and γ, and with k = 0 and K_d = 0.01. (*C*) Simulated dose–responses were fit to the Hill equation, and estimates for EC_{50} and Hill slope were computed for various τ, γ combinations. The Hill slope is uniquely determined by τ, such that for τ < 1, when the system is operating within an ultrasensitive regime, switch-like responses are observed. In the ultrasensitive regime, γ alone governs the EC_{50} of the dose–response.

parameter τ, such that hyperbolic-like responses occur at τ > 1, while ultrasensitive responses at τ < 1. As τ decreases relative to 1, the degree of ultrasensitivity increases; this is related to the Hill slope (n) of the ligand dose–response, such that τ < 1 corresponds to n > 1 (Fig. 5 *B* and *C*). The model explains the observed n ≈ 2 Hill slope for SMO regulation by wild-type PTCH1 in two ways. First, it suggests that PTCH1 acts as an enzyme to inhibit SMO and second that PTCH1 is saturated (i.e., τ < 1) and the system functions in an ultrasensitive regime.

The model shows that within the ultrasensitive regime (τ < 1) the Hill slope of the response to ligand is completely determined by τ, such that an arbitrarily small τ produces an arbitrarily large n. Thus, the elevated Hill slopes observed for Subset 1 of PTCH1 HPE mutants (Fig. 4 *A* and *D*) are likely due to changes in τ. Since τ is a function of PTCH1 Michaelis constant (K_M), it is likely that these mutants alter PTCH1 in such a way as to decrease its K_M. In the case of Subset 2 HPE mutants (Fig. 4*B*), the model suggests that they have higher γ than wild-type PTCH1. Since γ is a function of PTCH1 k_{cat}, it is likely that these mutants alter PTCH1 in such a way as to increase its catalytic activity toward active SMO. We note that the k parameter in Eq. 3, which determines the relative amount of SMO_C at maximal stimulation with ligand, does not vary significantly between wild-type PTCH1 and HPE mutants (Fig. 4 *A*–*C* and *SI Appendix*, Fig. S4 and *Supplementary Discussion*).

Finally, the model also explains why increases in Hill slope and EC_{50} are mutually exclusive (Fig. 4*D*). Within the ultrasensitive regime, changes in τ and γ have opposite effects on Hill slope and EC_{50}; decreases in τ increase Hill slope without affecting EC_{50}, while increases in γ increase EC_{50} without affecting Hill slope (Fig. 5*C*). This matches our observations (Fig. 4*D*), supporting ultrasensitivity as a fundamental feature of SMO regulation by PTCH1.

Defective SHH Binding Explains the Phenotype of One PTCH1 HPE Mutant. Uniquely among PTCH1 HPE mutants, V894G shows wild-type potency in repressing SMO (Fig. 1 *E* and *F* and *SI Appendix*, Fig. S1 *D* and *E*), suggesting that this mutant differs from the others in the mechanism by which it reduces Hh signaling. Indeed, PTCH1 V894G affinity for unpalmitoylated SHH is reduced by more than 100-fold (Fig. 6*A*), while affinity for the palm-SHH22 peptide is greatly reduced as well (Fig. 6*B*); thus, the V894G mutation impairs both the protein-dependent and the palmitate-dependent components of the PTCH1–SHH interaction. Consistent with this severe defect in binding, PTCH1 V894G has a greatly increased EC_{50} toward palm-SHH22 (Fig. 4 *B* and *D*), and SHH does not cause loss of PTCH1 V894G from cilia (*SI Appendix*, Fig. S3*G*). These data explain why the V894G mutant causes HPE while displaying normal inhibitory activity toward SMO. Interestingly, carriers of the V894G mutation showed a severe clinical phenotype: alobar HPE and microcephaly (28).

An Allosteric Mechanism for Defective SHH Binding by One PTCH1 HPE Mutant. Our results show that V894 is essential for PTCH1 binding to SHH; however, V894 is located far from PTCH1 surfaces that interact with SHH (32, 33) (Fig. 6*C*), raising the question of how V894 affects ligand binding. V894 lies within a short loop (F-loop) of PTCH1 ECD2 (30–33, 45) (Fig. 6 *C*–*E*). We find that other

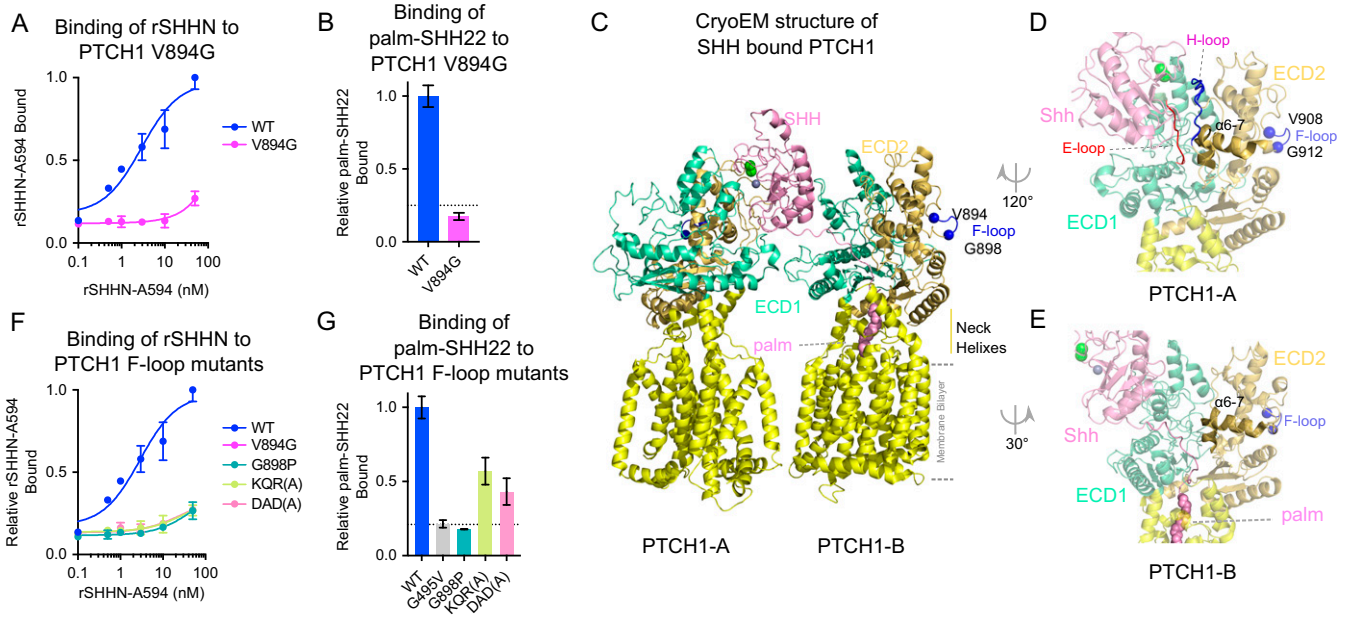

Fig. 6. A PTCH1 HPE mutant defective in binding and responding to SHH. (*A*) Wild-type and V894G PTCH1ΔC constructs were expressed in HEK293T cells, and saturation binding of rSHH-AlexaFluor594 was measured by fluorescence microscopy. The V894G mutant is defective in binding rSHH. Data show mean of two biological replicates with associated SDs; curves show binding isotherm fits. This measurement was performed together with the other HPE mutants (Fig. 4*D*), and wild-type PTCH1 data are duplicated in this panel for clarity. (*B*) As in *A*, but with binding of fluorescent palm-SHH22. V894G is defective for palm-SHH22 binding. (*C–E*) Cryo-EM structure of PTCH1 bound to palmitoylated SHH (Protein Data Bank ID code 6E1H; ref. 32). SHH (pink) binds two PTCH1 molecules simultaneously: PTCH1-A, which binds the SHH globular domain, and PTCH1-B, which binds the palmitoylated SHH N terminus (equivalent to palm-SHH22). The ECD2 F-loop (blue) harbors residues V894 and G898, which are necessary for ligand binding. (*D*) Connection between ECD2 F-loop, ECD2 α6–7 helixes, SHH-binding ECD1 E-loop (red) and ECD2 H-loop (blue). (*E*) Connection between ECD2 F-loop, ECD2 α6–7 helixes, and the PTCH1 "neck" helixes that bind the palmitoylated SHH N terminus. (*F*) As in *A*, but with binding to PTCH1 F-loop mutants. F-loop residues are necessary for binding the globular domain of SHH. (*G*) As in *B*, but with binding to PTCH1 F-loop mutants. F-loop residues are necessary for binding the palmitoylated SHH N terminus.

F-loop residues are also necessary for SHH binding: Mutating the highly conserved G898 has a similar effect to V894G (Fig. 6 *F* and *G*), while mutating less conserved residues (K890, Q891, R892, D894, and D896) has milder effects, abolishing SHH binding (Fig. 6*F*) but only reducing palm-SHH22 binding (Fig. 6*G*). Importantly, F-loop PTCH1 mutants localize to cilia (*SI Appendix*, Fig. S5*A*) and are fully active in repressing SMO (*SI Appendix*, Fig. S5*B*), indicating that they are properly folded and functional. Since the F-loop does not directly engage SHH, we propose that the ligand binding defect in F-loop mutants is explained by allosteric communication between the F-loop and the ligand-binding surfaces of PTCH1 (Fig. 6 *C–E* and *Discussion*).

PTCH1 Inhibits SMO by Antagonizing Cholesterol at the CRD. SMO harbors three distinct small-molecule binding sites (Fig. 7*A*): a sterol-binding site in the CRD (21, 25–28) and two sites in the 7TMD, one binding various synthetic modulators (29, 41) and another binding cholesterol (29). An unresolved issue is how these sites interact functionally and how they participate in SMO regulation by PTCH1 via cholesterol. To answer this question, we first measured activation of endogenous SMO by SAG in PTCH1-positive and PTCH1-negative cilia, using the single-cilia assay (Fig. 7 *B–D*). As shown in Fig. 7*C*, the EC_{50} for SAG is increased in the presence of PTCH1 (from 50 nM to 114 nM), a result consistent with Models 2 and 3, whereby PTCH1 activity increases SMO^R, thus requiring more SAG to activate SMO. Surprisingly, SMO activation by SAG is switch-like (Hill slope $n = 1.9 \pm 0.3$; Fig. 7*D*), with PTCH1 blunting the Hill slope (to $n = 1.3 \pm 0.2$; Fig. 7*D*). Given that SAG binds at a single 7TMD site, SMO activation by SAG would have been expected to have a Hill slope $n = 1$, unaffected by PTCH1. The $n \approx 2$ Hill slope and its dependence on PTCH1 suggests that SMO is activated cooperatively by SAG and endogenous cholesterol, as a result of allosteric coupling between the 7TMD SAG site and a cholesterol-binding site antagonized by PTCH1.

We asked whether the CRD cholesterol-binding site is involved in the cooperative activation of SMO by SAG, and in SMO regulation by PTCH1. We first compared the response to SAG of wild-type SMO and SMOΔCRD (Fig. 7 *E–G*), a construct lacking the CRD but still active in signaling (39). Dramatically, the Hill slope of the response of SMO to SAG drops from $n \approx 2$ to $n \approx 1$ when the CRD is deleted (Fig. 7*G*), confirming allosteric communication between the CRD cholesterol site and SAG 7TMD site. Importantly, the SAG EC_{50} for SMOΔCRD is greatly decreased compared to wild-type SMO (490 nM versus 16 nM; Fig. 7*F*), consistent with the elevated basal activity observed for SMOΔCRD (26, 28) and suggesting that in the absence of cholesterol the CRD represses the 7TMD. However, CRD deletion is not sufficient to fully activate SMO, as indicated by the fact that SMOΔCRD can still be activated by SAG; this suggests that, during Hh pathway stimulation, the CRD switches from repressing the 7TMD to activating it, in a cholesterol-dependent manner.

We next measured the effect of PTCH1 on SMO activation by 20(S)-hydroxycholesterol (20-OHC), a sterol agonist that acts exclusively through the CRD site (26, 28) (Fig. 7 *H–J*). The response of SMO to 20-OHC has a Hill slope $n \approx 1$ (Fig. 7*J*), indicating that sterol binding to the CRD activates SMO without cooperation with an endogenous 7TMD ligand. Furthermore, PTCH1 has no effect on the Hill slope (Fig. 7*J*), consistent with PTCH1 regulating SMO through the same CRD site bound by 20-OHC. Importantly, PTCH1 has only a modest effect on the EC_{50} of 20-OHC (3 μM; Fig. 7*I*), indicating that PTCH1 cannot efficiently antagonize 20-OHC–bound SMO; in contrast, PTCH1 antagonizes SMO activation by exogenous cholesterol (*SI Appendix*, Fig. S6).

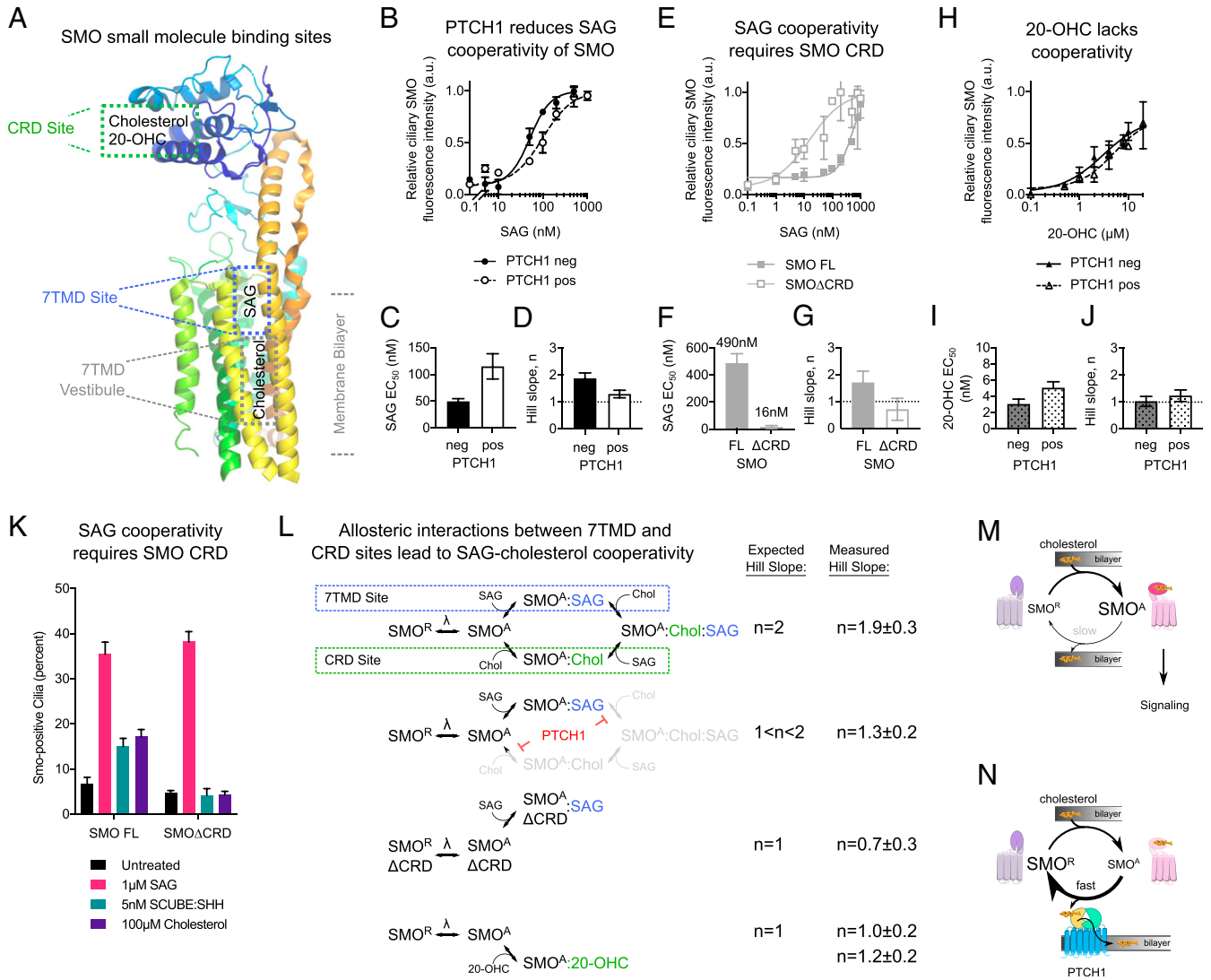

Fig. 7. PTCH1 represses SMO by antagonizing CRD cholesterol. (*A*) Structure of human SMO (Protein Data Bank ID code 6D35; ref. 42), showing location of the small-molecule binding sites in the CRD and 7TMD. (*B*) Ptch1$^{-/-}$ MEFs were transduced with a lentivirus expressing wild-type PTCH1-mCHERRY, but PTCH1 was not expressed in all cells. The cell population was treated with various doses of SAG for 6 h, and accumulation of endogenous SMO in PTCH1-positive and PTCH1-negative cilia was measured. Maximal ciliary SMO was determined by stimulation with saturating doses of both SHH and SAG (1 μM). Data show normalized median ciliary SMO intensity from two biological replicates, with associated SDs shown by error bars. Curves show least-squares fits to the Hill equation with minimum value 0.1 and maximum value 1. (*C* and *D*) EC_{50} and Hill slope parameter estimates from the curves in *B*; error bars show SE of the estimates. PTCH1 expression increases the EC_{50} and decreases the Hill slope of the response of endogenous SMO to SAG. (*E*) As in *B*, but with Smo$^{-/-}$ MEFs stably expressing mCHERRY-tagged wild-type SMO or SMOΔCRD and measuring ciliary levels of the mCHERRY signal. Data were analyzed and plotted as in *B*. (*F* and *G*) As in *C* and *D*, but for the curves in *E*. CRD deletion reduces the Hill slope of the response to SAG from n = 1.7 ± 0.4 to n = 0.7 ± 0.4, indicating that the CRD is required for switch-like activation of SMO by SAG. SMOΔCRD has a greatly reduced EC_{50} for SAG compared to wild-type SMO, consistent with higher basal activity of SMOΔCRD. (*H*) As in *B*, but assaying SMO activation by various doses of 20-OHC. Data were analyzed and plotted as in *B*. (*I* and *J*) As in *C* and *D*, but for the curves in *H*. PTCH1 expression does not affect the EC_{50} or Hill slope of the SMO response to 20-OHC. (*K*) As in *E*, but with the indicated doses of SAG, 20-OHC, MCD-cholesterol, or purified SCUBE2:SHH. SMOΔCRD does not respond to 20-OHC, MCD-cholesterol, and SCUBE2:SHH but reponds to SAG. In contrast, wild-type SMO responds to all activators. (*L*) Summary of allosteric interactions between SMO small-molecule binding sites. Cholesterol and SAG show cooperativity (Hill slope n = 2) because each binds active SMO (SMO^{A}) at independent, allosterically coupled sites (CRD and 7TMD). PTCH1 diminishes cooperativity (Hill slope 1 < n < 2) by reducing the occupancy of cholesterol at the CRD site. SAG activation of SMOΔCRD does not show cooperativity (Hill slope n = 1) because it lacks the CRD site. 20-OHC does not show cooperativity (Hill slope n = 1) because 20-OHC and cholesterol compete for binding to the CRD. (*M*) Model of PTCH1–SMO regulation. SMO undergoes an activation–inactivation equilibrium: cholesterol binding activates SMO, while slow spontaneous cholesterol dissociation causes SMO to return to its inactive state. Cholesterol binding occurs perhaps in the secretory pathway, before SMO reaches the cilium; as a result, this does not trigger the Hh pathway, because signal transduction downstream of SMO requires cilium-resident factors. (*N*) Active SMO translocates to the primary cilium, where it encounters PTCH1, which deactivates SMO by catalyzing cholesterol removal and deposition into the membrane bilayer, a process similar to cholesterol egress from lysosomes catalyzed by the Niemann–Pick disease Type-C proteins NPC2 and NPC1 (50, 51). Inactive SMO is removed from the cilium and can then undergo another activation event. If PTCH1 is inhibited or knocked out, active SMO accumulates in the cilium unimpeded and triggers downstream signaling.

Finally, we asked what the role is of the CRD in the response of SMO to exogenous sterols (which activate SMO directly) and to SHH (which activate SMO indirectly, by inhibiting PTCH1). As shown in Fig. 7*K*, in contrast to wild-type SMO, SMOΔCRD does not respond to sterols or to purified SCUBE2:SHH, indicating that the CRD is required for

SMO activation by sterols and for its cholesterol-dependent regulation by PTCH1.

Taken together, these data support the hypothesis that the CRD and 7TMD of SMO are allosterically coupled and that PTCH1 regulates SMO via cholesterol binding to the CRD (Fig. 7 *M* and *N*).

Discussion

PTCH1 represses SMO, thus ensuring the Hh pathway is off in the absence of the SHH ligand. SHH inhibits PTCH1, triggering SMO activation and Hh signal transduction. Interestingly, mutations in PTCH1 have been identified in human diseases with phenotypes characteristic of either constitutive of Hh signaling or insufficient Hh signaling. On the one hand, PTCH1 mutations are found in cancer; these are well-understood LOF mutations that impair the ability of PTCH1 to repress SMO, leading to constitutive SMO activation and excessive Hh signaling. On the other hand, PTCH1 mutations are found in HPE, a developmental defect characterized by insufficient Hh signaling; these mutations are poorly understood, and it is unknown if and how they reduce Hh signaling. Here, we use single-cell functional assays and mathematical modeling to understand how PTCH1 represses SMO and to determine how PTCH1 HPE mutations affect Hh signaling. We find that Hh pathway activation by SHH is switch-like, which can be attributed to PTCH1 inhibiting SMO like an enzyme operating close to saturation. Our results are consistent with a model whereby ciliary PTCH1 catalyzes deactivation of SMO, which is activated by cholesterol. Strikingly, all but one of the PTCH1 HPE mutants repress SMO more potently than wild-type PTCH1. These mutants are less responsive to SHH, although SHH binding is unaffected. Together, enhanced SMO repression and reduced responsiveness to SHH explain how these PTCH1 mutants dampen Hh signaling. The remaining PTCH1 HPE mutant (V894G) represses SMO normally but is severely impaired in binding SHH; this mutant likely causes HPE by simply being refractory to SHH. PTCH1 HPE mutants are thus all defective in responding to SHH, either by failing to bind it or because inhibition of hyperactive PTCH1 requires a larger amount of SHH.

That most PTCH1 HPE mutants are better than the wild type at repressing SMO raises an interesting question: Why has PTCH1 not naturally evolved to be more potent? We speculate that, since PTCH1 potency and responsiveness to SHH correlate inversely, potency should not be excessive, as this would require very high concentrations of SHH to trigger Hh signaling. Thus, PTCH1 potency must be balanced, to allow control by physiological ligand concentrations.

The switch-like response of wild-type PTCH1 to SHH (Hill coefficient $n \approx 2$) could be explained by either allostery or ultrasensitivity. Recent cryo-EM structures show SHH can bind simultaneously two PTCH1 molecules (32, 33), so coupling between PTCH1 protomers via Changeux–Wyman–Monod-type allostery (46) could conceivably account for $n \approx 2$. However, allosteric coupling within a PTCH1 dimer cannot explain the $n \approx 3$ observed for some HPE PTCH1 mutants. Furthermore, we observe an $n \approx 2$ for the response to the palmitoylated SHH peptide, which does not dimerize PTCH1, because it lacks the SHH globular domain. Thus zero-order ultrasensitivity is a likelier explanation for the switch-like activation of the Hh pathway.

Ultrasensitivity describes a response with $n > 1$, arising when an enzymatic activation–inactivation cycle operates near saturation (44). It has been proposed that PTCH1 represses SMO catalytically (39, 47), which is supported by our single-cell results. The τ parameter (Eq. 3) specifies the strength of the response: When $\tau > 1$ the system is not saturated and responds in a hyperbola-like manner ($n \approx 1$), while when $\tau < 1$ the system is near saturation and responds ultrasensitively ($n > 1$) (*SI Appendix, Supplementary Discussion*). The observed $n \approx 2$ thus suggests that PTCH1 is near saturation and the PTCH1–SMO module operates in an ultrasensitive regime. This is further supported by the behavior of PTCH1 HPE mutants. In an ultrasensitive regime the PTCH–SMO module should produce mutually exclusive changes in n and EC_{50} upon changes in τ and γ, respectively. Our data are consistent with this prediction: One set of HPE mutants (Set 1: V737A/G and T1038M) shows an increase in n but no change in EC_{50}, and another set (Set 2: A429G, S813G, and T714M) shows an increase in EC_{50} but not in n.

What do our results suggest about how PTCH1 inhibits SMO? At least two possibilities exist for PTCH1 function: 1) PTCH1 might prevent SMO activation (for example, by maintaining a cholesterol-poor environment in cilia) or 2) PTCH1 might stimulate SMO deactivation (for example, by depleting cholesterol from SMO). The first scenario is consistent with the two-step model of SMO activation (21), whereby ciliary localization and activation of SMO are separate events, occurring successively. This model relies on the fact that inactive SMO (SMO^R) can localize to cilia, as exemplified by overexpressed SMO (21) and by SMO bound to the antagonist cyclopamine (21, 22). More recently, however, SMO^R was found to enter the cilium much slower than active SMO (SMO^A) (48), suggesting that ciliary entry and activation are correlated, consistent with the second scenario above. Moreover, stable SMO overexpression always leads to some degree of Hh pathway activation (28), suggesting that cilia-localized SMO might, in fact, be active; this finding is also consistent with the second scenario and can be explained by SMO^A levels exceeding PTCH1 deactivation capacity. Finally, cyclopamine-bound SMO adopts a conformation (23) distinct from the inactive one (41) and similar to the fully active conformation (29), which might explain why it localizes to cilia despite not activating Hh signaling.

The results of our pharmacological cross-competition assay suggest that PTCH1 antagonizes both SMO activation and accumulation in cilia. Importantly, both SMO parameters are decreased for LOF PTCH1 mutants and increased for hyperactive HPE mutants. These results are consistent with the idea that only SMO^A enters the cilium and suggest that PTCH1 may act as a gatekeeper at the ciliary base (49), preventing SMO^A entry. Such a mechanism would imply that SMO binds cholesterol before reaching the cilium, in the secretory pathway; however, SMO^A cannot activate downstream signaling outside the cilium. We speculate that PTCH1 catalyzes removal of cholesterol from SMO^A, thus causing its conversion to SMO^R, which cannot enter the cilium (Fig. 7 *M* and *N*). Cholesterol might be directly transferred from SMO^A to PTCH1 via a transient interaction between the two proteins, similar to the handoff of cholesterol from NPC2 to NPC1 in lysosomes (50, 51); an attractive feature of this mechanism is its specificity, deriving from the PTCH1–SMO enzyme–substrate relationship. Alternatively, SMO^A deactivation might be promoted indirectly by PTCH1, perhaps via its proposed effect on cholesterol distribution between membrane leaflets (52, 53). Following deactivation, SMO^R can bind cholesterol again outside the cilium, shifting back to SMO^A. This activation–deactivation cycle can explain the PTCH1–SMO regulatory module produces ultrasensitivity.

How can hyperactivity of HPE mutants be rationalized if PTCH1 deactivates SMO? Changes in n and EC_{50} are directly correlated with changes in parameters τ and γ, such that decreases in τ are predicted to increase n, while increases in γ are predicted to increase EC_{50}. Thus, PTCH1 HPE mutants with elevated n (Set 1) may retune PTCH1–SMO regulation by decreasing τ, while PTCH1 HPE mutants with elevated EC_{50} (Set 2) may increase γ. Parameters τ and γ express the K_M and k_{cat} of the PTCH1 enzyme relative to total SMO. Because total SMO does not vary with PTCH1 expression, changes to τ or γ in HPE mutants can be attributed to changes in PTCH1 K_M or k_{cat}. We thus speculate that Set 1 mutants cause altered Hh signaling by

decreasing the K_M (i.e., increasing PTCH1 affinity for its SMO substrate), and that Set 2 mutants cause altered signaling by increasing the k_{cat} (i.e., speeding up SMO deactivation). Further studies are necessary to test these predictions, particularly determining biochemically if and how PTCH1 deactivates SMO.

Our results also shed light on the mechanism of SMO activation. We find that the SMO response to SAG has a Hill slope n $\approx$ 2, which is reduced by PTCH1 overexpression or by CRD deletion, indicating that SAG-bound 7TMD cooperates allosterically with cholesterol-bound CRD; this is consistent with previous pharmacological studies showing synergistic activation of SMO by SAG and 20-OHC (54). The effect of PTCH1 on the Hill slope can be explained by reducing cholesterol occupancy of the CRD, further underscoring the importance of this domain for SMO regulation by PTCH1. Interestingly, we find that CRD deletion sensitizes SMO to SAG, pointing to the additional role of the CRD in inhibiting SMO in the absence of Hh stimulation. Together, our results support the idea that the unliganded CRD represses the 7TMD, while cholesterol binding to the CRD relieves this repression and allosterically activates the 7TMD.

An unresolved question is how the recently described cholesterol binding site in the 7TMD (29) is regulated during Hh signaling. Since both this site (29) and the CRD are required for activation by SHH, perhaps SMO activation requires cholesterol binding to both the CRD and the 7TMD sites. In this scenario, PTCH1 inhibition by SHH leads to SMO allosteric activation by cholesterol binding to two distinct sites. Alternatively, the 7TMD cholesterol site is part of the conduit through which cholesterol moves from the membrane to the CRD during SMO activation (42). Our data (Fig. 7) favor the latter model.

PTCH1 binds both the lipidated ends of SHH as well as its globular domain (30–33, 45). The lone PTCH1 HPE mutant (V894G) that does not bind SHH or palm-SHH22 raises an interesting question: How can a mutation far from the PTCH1–ligand interaction interfaces have such a drastic ligand-binding defect? We find that the PTCH1 ECD2 F-loop, which includes V894, is necessary for ligand binding, indicating that the F-loop is allosterically coupled to the ligand-binding surfaces of PTCH1. A plausible path for this coupling is suggested by structures of SHH-bound PTCH1 (Fig. 6 *C*–*E*). The F-loop is connected through its C terminus with ECD2 helixes α6 and α7, which abut the H-loop of ECD2, which, in turn, contacts the E-loop of ECD1; the H- and E-loops form the binding site for the SHH globular domain (32, 33). Furthermore, ECD2 helixes α6 and α7 are near the PTCH1 juxtamembrane helixes that bind the palmitoyl moiety of SHH (31–33). These connections of the F-loop suggest how F-loop alterations might disrupt ligand interaction, via conformational changes in SHH-binding surfaces. We speculate that the surface-exposed F-loop could bind factors that modify PTCH1 sensitivity to ligand, thereby modulating Hh signaling.

Materials and Methods

Ciliary PTCH1 and SMO Measurements. Immunofluorescence images were acquired on an automated microscope (TE2000E; Nikon) equipped with a digital camera (OrcaER; Hamamatsu), using a 40× objective (Plan Apo 0.95 numerical aperture; Nikon). For quantifying ciliary localization, cilia were segmented based on ARL13B staining, and fluorescence intensities of PTCH1-mCHERRY and endogenous SMO at cilia were calculated using custom image analysis software implemented in ImageJ and MATLAB (MathWorks), as described (28). At least 300 cilia were quantified for each condition. Relative ciliary SMO was computed as the ratio of ciliary SMO intensity and the maximal amount of ciliary SMO (SMO_T), where SMO_T was defined as the median ciliary SMO fluorescence intensity in cells treated with SHH conditioned media and 0.1 μ SAG for 3 h. To determine PTCH1–SMO correlations (Fig. 1 *B*, *E*, and *F*), PTCH1 ciliary intensities were binned and median ciliary SMO fluorescence intensity was computed for each bin. Fluorescence-intensity thresholds used to define PTCH1-positive cilia were set as the 95th percentile of mCHERRY fluorescence in cilia of *Ptch1*$^{-/-}$ MEFs reconstituted with wild-type PTCH1 and treated with SHH conditioned media for 3 h. Fluorescence-intensity thresholds used to define SMO-positive cilia were set as the 95th percentile of SMO fluorescence in cilia of *Ptch1*$^{-/-}$ MEFs treated with 1 μM SANT1 for 3 h.

For detailed description of chemicals, antibodies, cell lines, protein, and peptide ligands see *SI Appendix*.

Regression Analysis. Fluorescence intensity data were imported into Prism 7 (GraphPad Software) and were fit using least-squares regression to the equations described in the text and *SI Appendix*.

Data Availability. All study data are included in the article and/or *SI Appendix*.

ACKNOWLEDGMENTS. We thank Hanna Tukachinsky and Yangqing Xu for helpful suggestions and discussions and Bradley Wierbowski for purified SCUBE2:SHH complex. This work was supported by NIH Grants R01 GM122920 and GM135262 to A.S.

1. P. W. Ingham, A. P. McMahon, Hedgehog signaling in animal development: Paradigms and principles. *Genes Dev.* **15**, 3059–3087 (2001).
2. L. Lum, P. A. Beachy, The hedgehog response network: Sensors, switches, and routers. *Science* **304**, 1755–1759 (2004).
3. P. Kruszka, M. Muenke, Syndromes associated with holoprosencephaly. *Am. J. Med. Genet. C. Semin. Med. Genet.* **178**, 229–237 (2018).
4. L. L. Rubin, F. J. de Sauvage, Targeting the Hedgehog pathway in cancer. *Nat. Rev. Drug Discov.* **5**, 1026–1033 (2006).
5. Y. Nakano *et al.*, A protein with several possible membrane-spanning domains encoded by the Drosophila segment polarity gene patched. *Nature* **341**, 508–513 (1989).
6. H. Nikaido, RND transporters in the living world. *Res. Microbiol.* **169**, 363–371 (2018).
7. J. Alcedo, M. Ayzenzon, T. Von Ohlen, M. Noll, J. E. Hooper, The Drosophila smoothened gene encodes a seven-pass membrane protein, a putative receptor for the hedgehog signal. *Cell* **86**, 221–232 (1996).
8. M. van den Heuvel, P. W. Ingham, Smoothened encodes a receptor-like serpentine protein required for hedgehog signalling. *Nature* **382**, 547–551 (1996).
9. D. T. Chang *et al.*, Products, genetic linkage and limb patterning activity of a murine hedgehog gene. *Development* **120**, 3339–3353 (1994).
10. Y. Echelard *et al.*, Sonic hedgehog, a member of a family of putative signaling molecules, is implicated in the regulation of CNS polarity. *Cell* **75**, 1417–1430 (1993).
11. S. Krauss, J. P. Concordet, P. W. Ingham, A functionally conserved homolog of the Drosophila segment polarity gene hh is expressed in tissues with polarizing activity in zebrafish embryos. *Cell* **75**, 1431–1444 (1993).
12. R. D. Riddle, R. L. Johnson, E. Laufer, C. Tabin, Sonic hedgehog mediates the polarizing activity of the ZPA. *Cell* **75**, 1401–1416 (1993).
13. L. V. Goodrich, M. P. Scott, Hedgehog and patched in neural development and disease. *Neuron* **21**, 1243–1257 (1998).
14. V. Marigo, R. A. Davey, Y. Zuo, J. M. Cunningham, C. J. Tabin, Biochemical evidence that patched is the Hedgehog receptor. *Nature* **384**, 176–179 (1996).
15. H. Tukachinsky, K. Petrov, M. Watanabe, A. Salic, Mechanism of inhibition of the tumor suppressor patched by sonic hedgehog. *Proc. Natl. Acad. Sci. U.S.A.* **113**, E5866–E5875 (2016).
16. B. M. Wierbowski *et al.*, Hedgehog pathway activation requires coreceptor-catalyzed, lipid-dependent relay of the Sonic hedgehog ligand. *Dev. Cell* **55**, 450–467.e8 (2020).
17. E. W. Humke, K. V. Dorn, L. Milenkovic, M. P. Scott, R. Rohatgi, The output of Hedgehog signaling is controlled by the dynamic association between Suppressor of Fused and the Gli proteins. *Genes Dev.* **24**, 670–682 (2010).
18. H. Tukachinsky, L. V. Lopez, A. Salic, A mechanism for vertebrate hedgehog signaling: Recruitment to cilia and dissociation of SuFu-Gli protein complexes. *J. Cell Biol.* **191**, 415–428 (2010).
19. D. Huangfu, K. V. Anderson, Cilia and Hedgehog responsiveness in the mouse. *Proc. Natl. Acad. Sci. U.S.A.* **102**, 11325–11330 (2005).
20. R. Rohatgi, L. Milenkovic, M. P. Scott, Patched1 regulates hedgehog signaling at the primary cilium. *Science* **317**, 372–376 (2007).
21. R. Rohatgi, L. Milenkovic, R. B. Corcoran, M. P. Scott, Hedgehog signal transduction by smoothened: Pharmacologic evidence for a 2-step activation process. *Proc. Natl. Acad. Sci. U.S.A.* **106**, 3196–3201 (2009).
22. C. W. Wilson, M.-H. Chen, P.-T. Chuang, Smoothened adopts multiple active and inactive conformations capable of trafficking to the primary cilium. *PLoS ONE* **4**, e5182 (2009).
23. P. Huang *et al.*, Cellular cholesterol directly activates smoothened in hedgehog signaling. *Cell* **166**, 1176–1187.e14 (2016).
24. G. Luchetti *et al.*, Cholesterol activates the G-protein coupled receptor Smoothened to promote Hedgehog signaling. *eLife* **5**, 1055 (2016).
25. E. F. X. Byrne *et al.*, Structural basis of Smoothened regulation by its extracellular domains. *Nature* **535**, 517–522 (2016).
26. B. R. Myers *et al.*, Hedgehog pathway modulation by multiple lipid binding sites on the smoothened effector of signal response. *Dev. Cell* **26**, 346–357 (2013).
27. S. Nachtergaele *et al.*, Structure and function of the Smoothened extracellular domain in vertebrate Hedgehog signaling. *eLife* **2**, e01340 (2013).

28. D. Nedelcu, J. Liu, Y. Xu, C. Jao, A. Salic, Oxysterol binding to the extracellular domain of Smoothened in Hedgehog signaling. *Nat. Chem. Biol.* **9**, 557–564 (2013).
29. I. Deshpande *et al*., Smoothened stimulation by membrane sterols drives Hedgehog pathway activity. *Nature* **571**, 284–288 (2019).
30. X. Gong *et al*., Structural basis for the recognition of sonic hedgehog by human Patched1. *Science* **361**, eaas8935 (2018).
31. X. Qi, P. Schmiege, E. Coutavas, J. Wang, X. Li, Structures of human Patched and its complex with native palmitoylated sonic hedgehog. *Nature* **560**, 128–132 (2018).
32. X. Qi, P. Schmiege, E. Coutavas, X. Li, Two Patched molecules engage distinct sites on Hedgehog yielding a signaling-competent complex. *Science* **362**, eaas8843 (2018).
33. H. Qian *et al*., Inhibition of tetrameric patched1 by sonic hedgehog through an asymmetric paradigm. *Nat. Commun.* **10**, 2320–2329 (2019).
34. K. Petrov, B. M. Wierbowski, J. Liu, A. Salic, Distinct cation gradients power cholesterol transport at different key points in the hedgehog signaling pathway. *Dev. Cell* **55**, 314–327.e7 (2020).
35. M. Athar, C. Li, A. L. Kim, V. S. Spiegelman, D. R. Bickers, Sonic hedgehog signaling in Basal cell nevus syndrome. *Cancer Res.* **74**, 4967–4975 (2014).
36. L. A. Ribeiro, J. C. Murray, A. Richieri-Costa, PTCH mutations in four Brazilian patients with holoprosencephaly and in one with holoprosencephaly-like features and normal MRI. *Am. J. Med. Genet. A.* **140**, 2584–2586 (2006).
37. J. E. Ming *et al*., Mutations in PATCHED-1, the receptor for SONIC HEDGEHOG, are associated with holoprosencephaly. *Hum. Genet.* **110**, 297–301 (2002).
38. L. V. Goodrich, L. Milenković, K. M. Higgins, M. P. Scott, Altered neural cell fates and medulloblastoma in mouse patched mutants. *Science* **277**, 1109–1113 (1997).
39. J. Taipale, M. K. Cooper, T. Maiti, P. A. Beachy, Patched acts catalytically to suppress the activity of Smoothened. *Nature* **418**, 892–897 (2002).
40. J. K. Chen, J. Taipale, K. E. Young, T. Maiti, P. A. Beachy, Small molecule modulation of Smoothened activity. *Proc. Natl. Acad. Sci. U.S.A.* **99**, 14071–14076 (2002).
41. C. Wang *et al*., Structural basis for Smoothened receptor modulation and chemoresistance to anticancer drugs. *Nat. Commun.* **5**, 4355 (2014).
42. P. Huang *et al*., Structural basis of smoothened activation in hedgehog signaling. *Cell* **174**, 312–324.e16 (2018).
43. C. M. Rominger *et al*., Evidence for allosteric interactions of antagonist binding to the smoothened receptor. *J. Pharmacol. Exp. Ther.* **329**, 995–1005 (2009).
44. J. E. Ferrell Jr, S. H. Ha, Ultrasensitivity part I: Michaelian responses and zero-order ultrasensitivity. *Trends Biochem. Sci.* **39**, 496–503 (2014).
45. A. F. Rudolf *et al*., The morphogen Sonic hedgehog inhibits its receptor Patched by a pincer grasp mechanism. *Nat. Chem. Biol.* **15**, 975–982 (2019).
46. J. Monod, J. Wyman, J. P. Changeux, On the nature of allosteric transitions: A plausible model. *J. Mol. Biol.* **12**, 88–118 (1965).
47. N. Denef, D. Neubüser, L. Pérez, S. M. Cohen, Hedgehog induces opposite changes in turnover and subcellular localization of patched and smoothened. *Cell* **102**, 521–531 (2000).
48. J. Kim *et al*., Simultaneous measurement of smoothened entry into and exit from the primary cilium. *PLoS One* **9**, e104070 (2014).
49. L. Milenkovic *et al*., Single-molecule imaging of Hedgehog pathway protein Smoothened in primary cilia reveals binding events regulated by Patched1. *Proc. Natl. Acad. Sci. U.S.A.* **112**, 8320–8325 (2015).
50. H. J. Kwon *et al*., Structure of N-terminal domain of NPC1 reveals distinct subdomains for binding and transfer of cholesterol. *Cell* **137**, 1213–1224 (2009).
51. X. Li *et al*., 3.3 Å structure of Niemann-Pick C1 protein reveals insights into the function of the C-terminal luminal domain in cholesterol transport. *Proc. Natl. Acad. Sci. U.S.A.* **114**, 9116–9121 (2017).
52. Y. Zhang *et al*., Structural basis for cholesterol transport-like activity of the hedgehog receptor patched. *Cell* **175**, 1352–1364.e14 (2018).
53. M. Kinnebrew *et al*., Cholesterol accessibility at the ciliary membrane controls hedgehog signaling. *eLife* **8**, e50051 (2019).
54. S. Nachtergaele *et al*., Oxysterols are allosteric activators of the oncoprotein smoothened. *Nat. Chem. Biol.* **8**, 211–220 (2012).